DET NORSKE VIDENSKAPS-AKADEMI I OSLO

GEOFYSISKE PUBLIKASJONER

GEOPHYSICA NORVEGICA

Vol. XXVII. No. 1 December 1967

ARNE GRAMMELTVEDT

On the nonlinear computational instability of the equations of one-dimensional flow

OSLO 1967
UNIVERSITETSFORLAGET

GEOFYSISKE PUBLIKASJONER
GEOPHYSICA NORVEGICA
VOL. XXVII NO. 1

ON THE NONLINEAR COMPUTATIONAL INSTABILITY OF THE EQUATIONS OF ONE-DIMENSIONAL FLOW[1]

By Arne Grammeltvedt

FREMLAGT I VIDENSKAPS-AKADEMIETS MØTE DEN 24. FEBRUAR 1967 AV ELIASSEN

Summary. The equations for a one-dimensional, homogeneous, incompressible, and hydrostatic fluid describing external gravity oscillations are integrated with different finite difference schemes which smooth the solutions in different ways. Only two of the schemes, one conserving total momentum in space and one conserving total energy in space, behave numerically stable up to 80 days.

The spectral equations corresponding to some of the schemes show that in the stable schemes the shortest waves are continuously damped, and the aliasing terms are small, but in the unstable schemes the dampening is small, and the aliasing errors and bad approximations to the wave numbers in the non-linear terms will make the solutions more unstable.

1. Introduction. Integration of the nonlinear initial-value problems in fluid dynamics and meteorology by numerical methods often introduces nonlinear instability from the nonlinear terms of the equations. Phillips (1959), Arakawa (1963), Lilly (1965), and Bryan (1966) have developed finite difference methods for long-term integrations which are nonlinearly stable, by using quadratic conserving forms of the advection terms. To make short and medium term integrations numerically stable, different methods have been used. Shuman (1957) and Phillips (1959) smoothed the dependent variables after a given number of timesteps; but using a smoothing operator is always time consuming, and it is more convenient to include the smoothing in the finite difference forms by averaging the dependent variables over different grid points or by introducing artificial friction to damp the shortest wave lengths, which are most computationally unstable. Shuman (1960) has made a study of the nonlinear computational instability of various finite difference forms of the equations describing the one-dimensional motion of a homogeneous incompressible fluid and found that only two of them, the semi-momentum form, which is a quadratic conserving form, and the filtered factor form, which includes continuous smoothing, were computationally

[1] This research has been sponsored by the Air Force Cambridge Research Laboratories through the European Office of Aerospace Research, OAR, United States Air Force, under Contract AF 61(052)–897.

stable for short and medium term integrations. An artificial friction is incorporated in the finite difference formulation of LAX and WENDROFF (1960) and in the "Euler-Cauchy" form of A. ELIASSEN (1964). The friction coefficients are here determined by the finite difference forms; but to study the influence of friction on the nonlinear instability, an addition of a friction term to the equation of motion, where we have the possibility of varying the friction coefficient, seems to be more realistic.

Integration of multi-level primitive equation models of the atmosphere indicates that the nonlinear instability occurs after 200—400 timesteps, when quadratic-conserving forms or smoothing are not used. The instability is on the shortest wave lengths and shows first in the most convergent zones of the flow. This analysis is an attempt to see if nonlinear instability in a divergent flow may be suppressed by smoothing the advection field or by including friction in the equation of motion.

2. The model. The model used in this study is the same as used by SHUMAN (1960), a one-dimensional, homogeneous, incompressible, and hydrostatic fluid. The equations for this model are

$$\frac{\partial u}{\partial t}=-u\frac{\partial u}{\partial x}-\frac{\partial h}{\partial x} \tag{2.1}$$

$$\frac{\partial h}{\partial t}=-\frac{\partial}{\partial x}(hu) \tag{2.2}$$

where t and x denote the time and space variables. $u=u(x, t)$ is the speed of the fluid and $h=gz$ is the potential of the fluid where g is the acceleration of gravity, and $z=z(x, t)$ the depth. The flow is assumed to be periodic in the x-direction with wave length L; $u(x)=u(x+L)$ and $h(x)=h(x+L)$. From (2.1) and (2.2) it follows that total mass

$$M=\int_0^L \frac{\rho}{g}h\,dx\,,$$

total momentum

$$B=\int_0^L \frac{\rho}{g}hu\,dx\,,$$

and total energy

$$E=\int_0^L \frac{\rho h}{2g}(u^2+h)\,dx$$

are conserved in this model, where ρ is a constant density.

To control the nonlinear computational instability three different kinds of smoothing have been used. First a friction term of the Fickian type is added to (2.1), and instead of (2.1) we get

$$\frac{\partial u}{\partial t}=-u\frac{\partial u}{\partial x}-\frac{\partial h}{\partial x}+\nu\frac{\partial^2 u}{\partial x^2} \tag{2.3}$$

where ν is the kinematic coefficient of viscosity.

Secondly the velocity is smoothed after each time step Δt, and (2.1) and (2.2) may be written

$$\frac{\partial u}{\partial t}=-\bar{u}\frac{\partial \bar{u}}{\partial x}-\frac{\partial h}{\partial x} \tag{2.4}$$

$$\frac{\partial h}{\partial t}=-\bar{u}\frac{\partial h}{\partial x}-h\frac{\partial \bar{u}}{\partial x} \tag{2.5}$$

where

$$\bar{u}=u+\beta\frac{\partial^2 u}{\partial x^2}$$

and β a smoothing coefficient.

Thirdly, nonlinear friction terms, where the friction coefficients are proportional to $\partial u/\partial x$ and $\partial h/\partial x$, are added to (2.1) and (2.2), and the equations become

$$\frac{\partial u}{\partial t}=-\left(u+\alpha\frac{\partial^2 u}{\partial x^2}\right)\frac{\partial u}{\partial x}-\frac{\partial h}{\partial x} \tag{2.6}$$

$$\frac{\partial h}{\partial t}=-\left(u+\alpha\frac{\partial^2 u}{\partial x^2}\right)\frac{\partial h}{\partial x}-\left(h+\alpha\frac{\partial^2 h}{\partial x^2}\right)\frac{\partial u}{\partial x} \tag{2.7}$$

3. Difference equations and stability considerations. The values of $u(x, t)$ and $h(x, t)$ in the point $x=j\Delta x$ and $t=r\Delta t$ are denoted by u_j^r and h_j^r, where j and r are integers, Δx is the space increment, and Δt is the time increment. The derivatives at the point (x, t) are approximated by

$$\frac{\partial u_j^r}{\partial t}\approx\frac{1}{2\Delta t}(u_j^{r+1}-u_j^{r-1}) \tag{3.1}$$

$$\frac{\partial u_j^r}{\partial x}\approx\frac{1}{2\Delta x}(u_{j+1}^r-u_{j-1}^r) \tag{3.2}$$

$$\frac{\partial^2 u_j^r}{\partial x^2}\approx\frac{1}{(\Delta x)^2}(u_{j+1}^r+u_{j-1}^r-2u_j^r) \tag{3.3}$$

and the same for h_j^r.

To simplify the difference equations the following nondimensional variables are used;

$$r = \frac{t}{\Delta t}$$

$$j = \frac{x}{\Delta x}$$

$$u' = u\frac{\Delta t}{\Delta x}$$

$$h' = h\left(\frac{\Delta t}{\Delta x}\right)^2$$

$$\nu' = \nu\frac{2\Delta t}{(\Delta x)^2}$$

$$\beta' = \beta\frac{1}{(\Delta x)^2}$$

$$\alpha' = \alpha\frac{1}{(\Delta x)^2}$$

The difference equation for (2.3), (2.2), (2.6), and (2.7) in the point (r, j) may then be written

$$u_j'^{r+1} = u_j'^{r-1} - u_j'^r(u_{j+1}'^r - u_{j-1}'^r) - (h_{j+1}'^r - h_{j-1}'^r) + \nu'(u_{j+1}'^r + u_{j-1}'^r - 2u_j'^r) \tag{3.4}$$

$$h_j'^{r+1} = h_j'^{r-1} - u_j'^r(h_{j+1}'^r - h_{j-1}'^r) - h_j'^r(u_{j+1}'^r - u_{j-1}'^r) \tag{3.5}$$

$$u_j'^{r+1} = u_j'^{r-1} - (u_j'^r + \alpha'(u_{j+1}'^r + u_{j-1}'^r - 2u_j'^r))(u_{j+1}'^r - u_{j-1}'^r) - (h_{j+1}'^r - h_{j-1}'^r) \tag{3.6}$$

$$\begin{aligned} h_j'^{r+1} = h_j'^{r-1} &- (u_j'^r + \alpha'(u_{j+1}'^r + u_{j-1}'^r - 2u_j'^r)(h_{j+1}'^r - h_{j-1}'^r) \\ &- (h_j'^r + \alpha'(h_{j+1}'^r + h_{j-1}'^r - 2h_j'^r))(u_{j+1}'^r - u_{j-1}'^r) \end{aligned} \tag{3.7}$$

The difference equation for (2.4) and (2.5) will be equal to (3.6) and (3.7) with $\alpha' = 0$ and $u'^r =$ replaced by $\bar{u}_j'^r$ where

$$\bar{u}_j'^r = u_j'^r + \beta'(u_{j+1}'^r + u_{j-1}'^r - 2u_j'^r) \tag{3.8}$$

As a starting point in the numerical integration a simple forward timestep is used. For the first timestep, (3.4a) is then used instead of (3.4):

$$\begin{aligned} u_j'^{r+1} = \tfrac{1}{2}(u_{j+1}'^r + u_{j-1}'^r) - \tfrac{1}{2}u_j'^r(u_{j+1}'^r - u_{j-1}'^r) \\ - \tfrac{1}{2}(h_{j+1}'^r - h_{j-1}'^r) - \frac{\nu'}{2}(u_{j+1}'^r + u_{j-1}'^r - 2u_j'^r) \end{aligned} \tag{3.4a}$$

and corresponding equations for the other variables.

The stability conditions, in the von Neumann sense, for these equations are assumed to be the same as the stability conditions for the linearized equations corresponding to them (see LAX and WENDROFF, 1960). The linearized equations corresponding to (3.4) and (3.5) are, when the primes are omitted,

$$u_j^{r+1}=u_j^{r-1}-u(u_{j+1}^r-u_{j-1}^r)-c(h_{j+1}^r-h_{j-1}^r)+\nu(u_{j+1}^r+u_{j-1}^r-2u_j^{r-1}) \tag{3.9}$$

$$h_j^{r+1}=h_j^{r-1}-u(h_{j+1}^r-h_{j-1}^r)-c(u_{j+1}^r-u_{j-1}^r) \tag{3.10}$$

where

$$u=\bar{u}\frac{\Delta t}{\Delta x}$$

and

$$c=\sqrt{gH}\,\frac{\Delta t}{\Delta x}$$

$\bar{u}$ is an average velocity and H an average depth of the fluid. When $\nu=0$, these equations are numerically stable if

$$|U|+C\leqslant 1 \tag{3.11}$$

where U and C are the maximum values of u and c.

To find the stability conditions for (3.4) and (3.5) let us first look at the equation

$$\frac{\partial u}{\partial t}=\nu\frac{\partial^2 u}{\partial x^2}. \tag{3.12}$$

As shown by MIYAKODA (1962), one stable difference approximation for (3.12) is

$$u_j^{r+1}=u_j^{r-1}+\nu(u_{j+1}^{r-1}+u_{j-1}^{r-1}-2u_j^{r-1}) \tag{3.13}$$

where the friction term is calculated at the time $r-1$.

If we substitute the Fourier term $u^r e^{i\kappa j\Delta x}$ for u_j^r into (3.13), where κ denotes wave number, the equation becomes

$$u^{r+1}=u^{r-1}\left(1-4\nu\sin^2\frac{\kappa\Delta x}{2}\right), \tag{3.14}$$

and the stability condition is

$$\left|1-4\nu\sin^2\frac{\kappa\Delta x}{2}\right|\leqslant 1$$

or

$$\nu\leqslant\tfrac{1}{4}$$

Another stable approximation for (3.12) is the difference equation

$$u_j^{r+1}=u_j^{r-1}+\nu(u_{j+1}^r+u_{j-1}^r-2u_j^{r-1}) \tag{3.15}$$

where u at $j+1$ and $j-1$ is taken at the time r, and u at j is taken at the time $r-1$. Let us introduce a new dependent variable $v_j^r=u_j^{r-1}$. (3.15) may then be written

$$\begin{aligned} u_j^{r+1}&=(1-2\nu)v_j^r+\nu(u_{j+1}^r+u_{j-1}^r)\\ v_j^{r+1}&=u_j^r\,. \end{aligned} \tag{3.16}$$

Substituting the Fourier terms $u^r e^{i\kappa j\Delta x}$ and $v^r e^{i\kappa j\Delta x}$ for u_j^r and v_j^r into (3.16) the following matrix form of the equations is derived

$$\begin{pmatrix} u^{r+1}\\ v^{r+1}\end{pmatrix}=A\begin{pmatrix} u^r\\ v^r\end{pmatrix} \tag{3.17}$$

where

$$A=\begin{pmatrix} 2\nu\cos\kappa\Delta x & 1-2\nu\\ 1 & 0\end{pmatrix}.$$

The eigenvalues of A are

$$\lambda_{1,2}=\nu\cos\kappa\Delta x\pm\sqrt{(\nu\cos\kappa\Delta x)^2+1-2\nu}\,. \tag{3.18}$$

The stability requires that the magnitude of the eigenvalues do not exceed unity, which establishes the stability condition

$$\nu<\tfrac{1}{2}$$

To find the stability condition for (3.9) and (3.10) we may write the equations in matrix form. By introducing two new dependent variables $v_j^r=u_j^{r-1}$ and $g_j^r=h_j^{r-1}$ and substituting u_j^r by the Fourier terms $u^r e^{i\kappa j\Delta x}$ and the same for v_j^r, u_j^r, and g_j^r, the equations are

$$\begin{pmatrix} u^{r+1}\\ v^{r+1}\\ h^{r+1}\\ g^{r+1}\end{pmatrix}=D\begin{pmatrix} u^r\\ v^r\\ h^r\\ g^r\end{pmatrix} \tag{3.19}$$

where

$$D=\begin{pmatrix} -2(iu\sin\kappa\Delta x-\nu\cos\kappa\Delta x) & 1-2\nu & -2ic\sin\kappa\Delta x & 0\\ 1 & 0 & 0 & 0\\ -2ic\sin\kappa\Delta x & 0 & -2iu\sin\kappa\Delta x & 1\\ 0 & 0 & 1 & 0\end{pmatrix}$$

The eigenvalues of the matrix D may be found numerically. Fig. 1 shows the domain of stability in a $(|u|, c)$ plane for various values of ν. The results are directly comparable with the results found by HOUGHTON *et al.*, (1966).

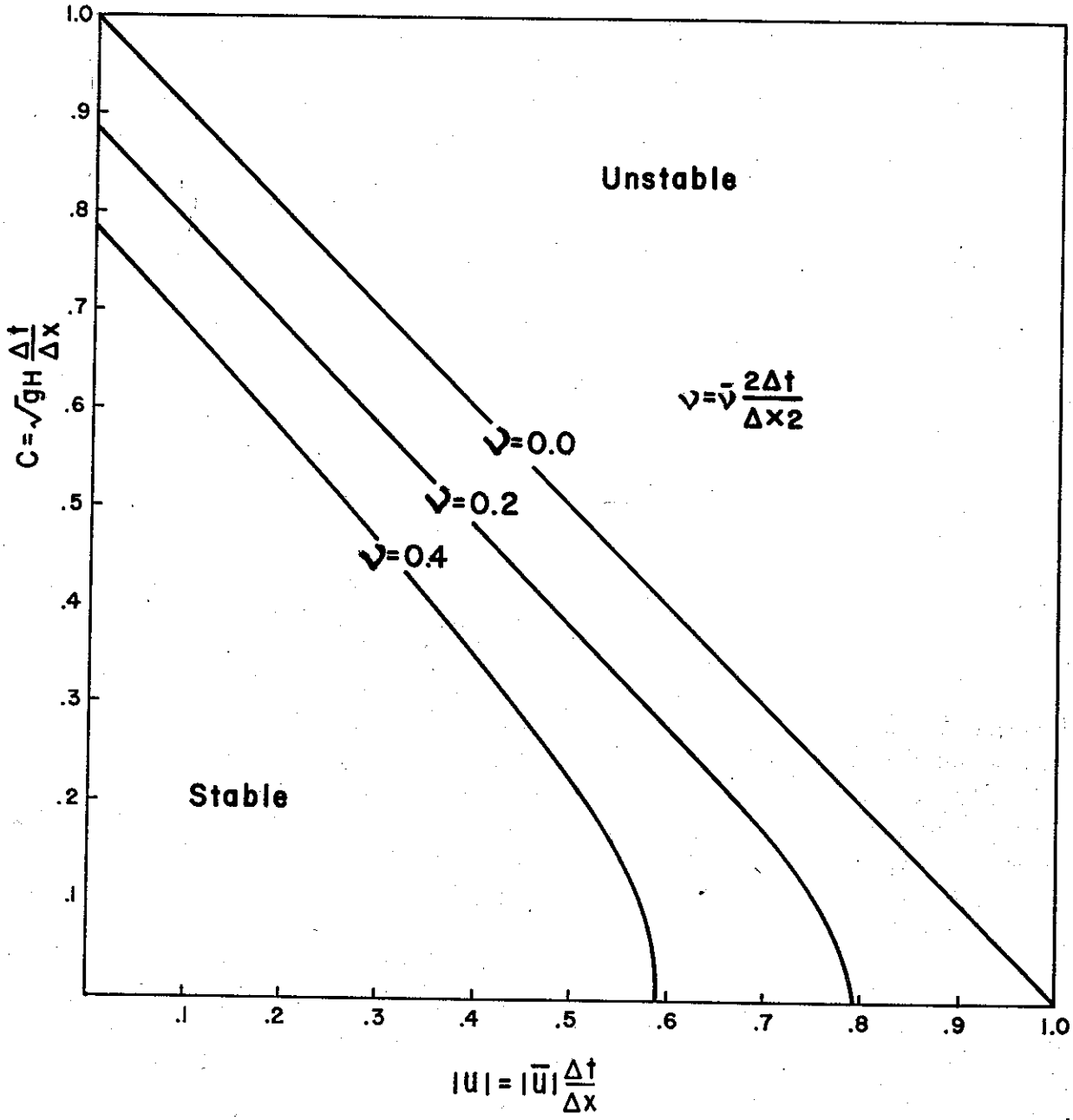

Fig. 1. The domain of stability for $\nu = 0.0$, $\nu = 0.2$ and $\nu = 0.4$ shown on a $(|u|, c)$ plane. $\nu = 0.1$ corresponds in dimensional form to $1.6 \cdot 10^7 \mathrm{m^2 sec^{-1}}$.

4. Initial conditions. In this study we will use the following initial conditions

$$u_j^r = \sum_{n=1}^{N} \hat{u}_n^r \sin nj\Delta x \tag{4.1}$$

and

$$h_j^r = \sum_{n=0}^{N} \hat{h}_n^r \cos nj\Delta x \tag{4.2}$$

With these initial conditions it follows from the Fourier analysis in chapter 6 that the velocity u_j^r will always consist of a sum of sine functions in x and the potential h_j^r a sum of consine functions in x. The total momentum in the region L will therefore always be zero for all the integration experiments. In the calculation the following values are adopted

$$\hat{u}_1 = 0.075$$

$$\hat{u}_n = 0 \qquad n = 2, 3 \ldots N$$

$$\hat{h}_0 = 0.18$$

$$\hat{h}_n = 0 \qquad n = 1, 2 \ldots N$$

$$\Delta t = 6 \text{ minutes}$$

$$\Delta x = 240 \text{ km}$$

$$L = 40\Delta x$$

$$N = \frac{L}{2\Delta x} = 20$$ (the total number of wave components in the model.)

5. Results. To find the nonlinear instability of the difference equations the total energy is calculated from (5.3), and the kinetic and potential energy of the different wave components are found by a Fourier analysis of u_j^r and h_j^r.

Equations (3.4) and (3.5) are integrated for 1500 timesteps, corresponding to 6 days, with different values of the kinematic eddy viscosity coefficient ν. The values of ν used are: $\nu = 0.01$, $\nu = 0.05$, and $\nu = 0.1$ (in units $(\Delta x)^2/2\Delta t = 0.8 \times 10^8$ m^2 sec^{-1}).

The results are given in Fig. 2.

For $\nu = 0.01$ the total energy decreases in the first 300 timesteps, but the dampening of the energy of the high wave numbers is not strong enough and nonlinear instability develops. If ν is increased to 0.05 the total energy decreases rapidly and after 800 timesteps the total energy is only 1/10 of its initial value, but after 1200 timesteps the energy again starts to increase. The same happens for $\nu = 0.1$, even if the available energy has been very small.

In the next experiment the velocity field is smoothed after each timestep by using different values of β in (3.8). The results are given in Fig. 3.

The results in Fig. 3 coincide well with the results in Fig. 2, and in a divergent flow it seems to be impossible to get rid of the nonlinear instabilities by using linear friction or by smoothing the velocity field without damping the available energy considerably.

Equations (3.6) and (3.7) are then integrated with $\alpha = 0$, 1/8, 1/6, 1/5, 1/4, 1/3, and 1/2. $\alpha = 0$ corresponds to Shuman's advective form, $\alpha = 1/4$ to the filter factor form, and $\alpha = 1/2$ to the semi-momentum form (SHUMAN, 1960). $\alpha = 1/3$ is a total momentum conservation form in space which gives

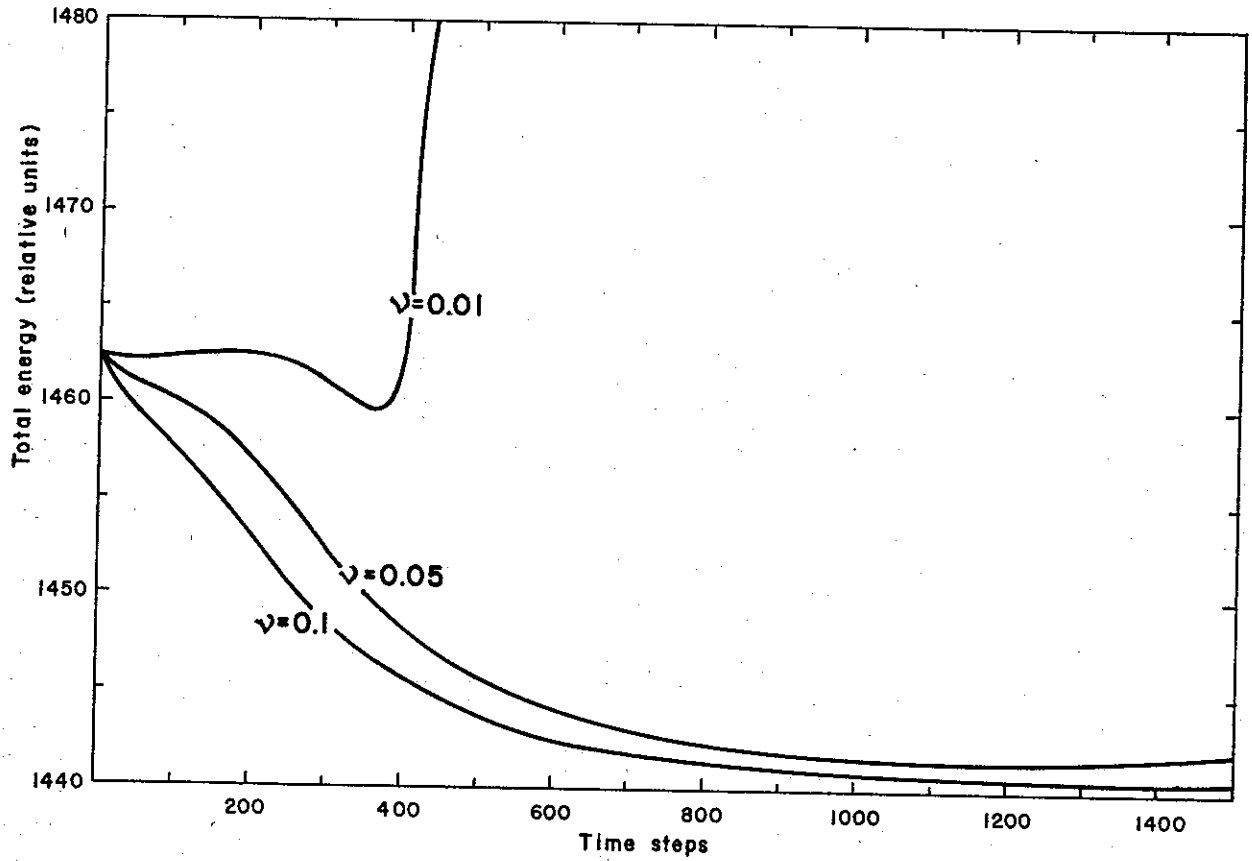

Fig. 2. Total energy variation in time for different friction coefficients.

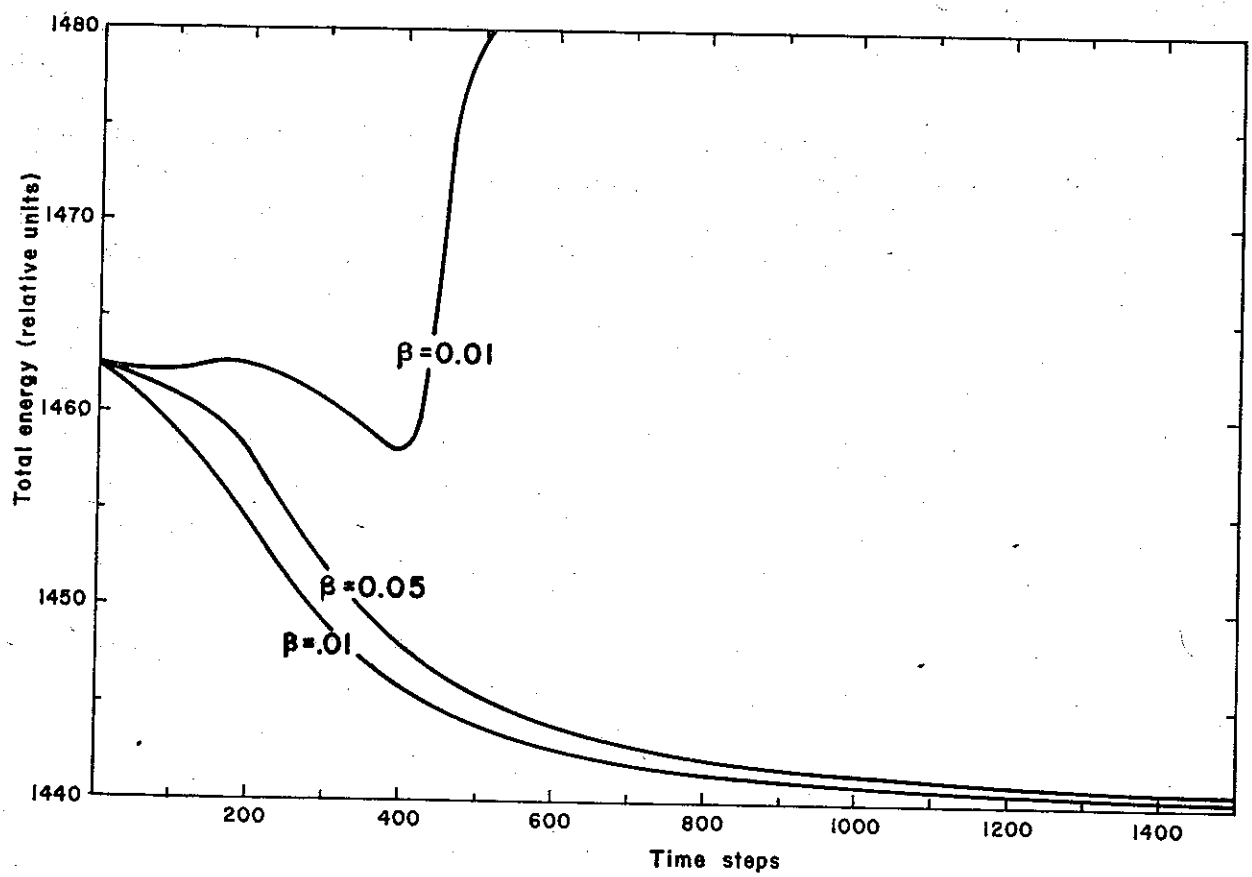

Fig. 3. Total energy variation in time for different smoothing coefficients.

$$\frac{\partial B}{\partial t}=\frac{\partial}{\partial t}\left(\sum_j u_j^r h_j^r\right)=0 \tag{5.1}$$

and the semi momentum form is a total energy conserving form in space for this model, which gives

$$\frac{\partial E}{\partial t}=\frac{\partial}{\partial t}\left(\sum_j \tfrac{1}{2}(u_j^{r2} h_j^r + h_j^{r2})\right)=0 \tag{5.2}$$

In Table 1 is shown the time of occurrence of the computational instability for different values of α, and we see that we have to choose $\alpha \geqslant 1/4$ to integrate (3.6) and (3.7) for more than 800 timesteps, corresponding to little more than 3 days. These results are the same as those found by Shuman.

Table 1. *Occurrence of computational instability*

α	Number of time steps	
0	350	
1/8	500	not useful
1/6	650	
1/5	800	
1/4	6000	
1/3	>20000	useful
1/2	>20000	

In the linearized system corresponding to (3.6) and (3.7) we might for each wave component have one real physical mode and one spurious computational mode if this is not eliminated by the initial conditions. The computational mode will give a spurious single timestep oscillation of the real solution of u_j^r and h_j^r and also of the total energy

$$E=\tfrac{1}{2}\sum_j (u_j^{r2} h_j^r + h_j^{r2}) \tag{5.3}$$

(MIKYAKODA, 1962; LILLY, 1965).

If we look at the energy distribution in time for the nonlinearized system (3.6) and (3.7) we have for all α's spurious oscillation of the energy with not only the single timestep frequency, but also of lower frequencies. As long as the solutions are stable the amplitude of these oscillations is small, but when we integrate for a very long time, the amplitude seems to increase with time.

The advective form, $\alpha=0$, becomes unstable after 350 timesteps. Fig. 4a shows the value of the potential, h, and the velocity, u, of the fluid at that time. (The potential is symmetric about the midpoint, and the velocity is asymmetric about the midpoint so only the right and the left halves of the curves are drawn.) The solid curve is drawn

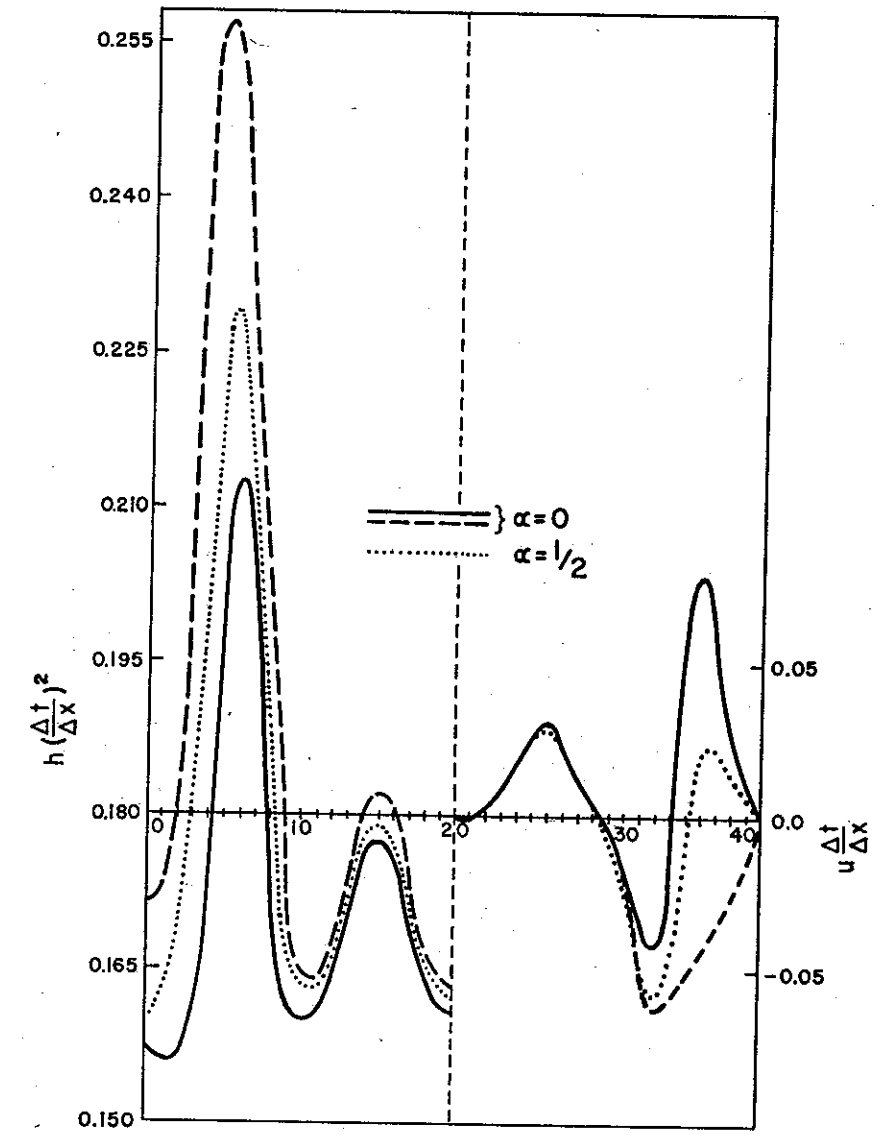

Fig. 4 (a) The potentials and the velocities and (b) the total energy distributions for $\alpha = 0$ and $\alpha = 1/2$ after 350 time-steps. (For $\alpha = 0$ the solid curve in Fig. (a) is drawn through the even gridpoints and the broken curve through the odd gridpoints.)

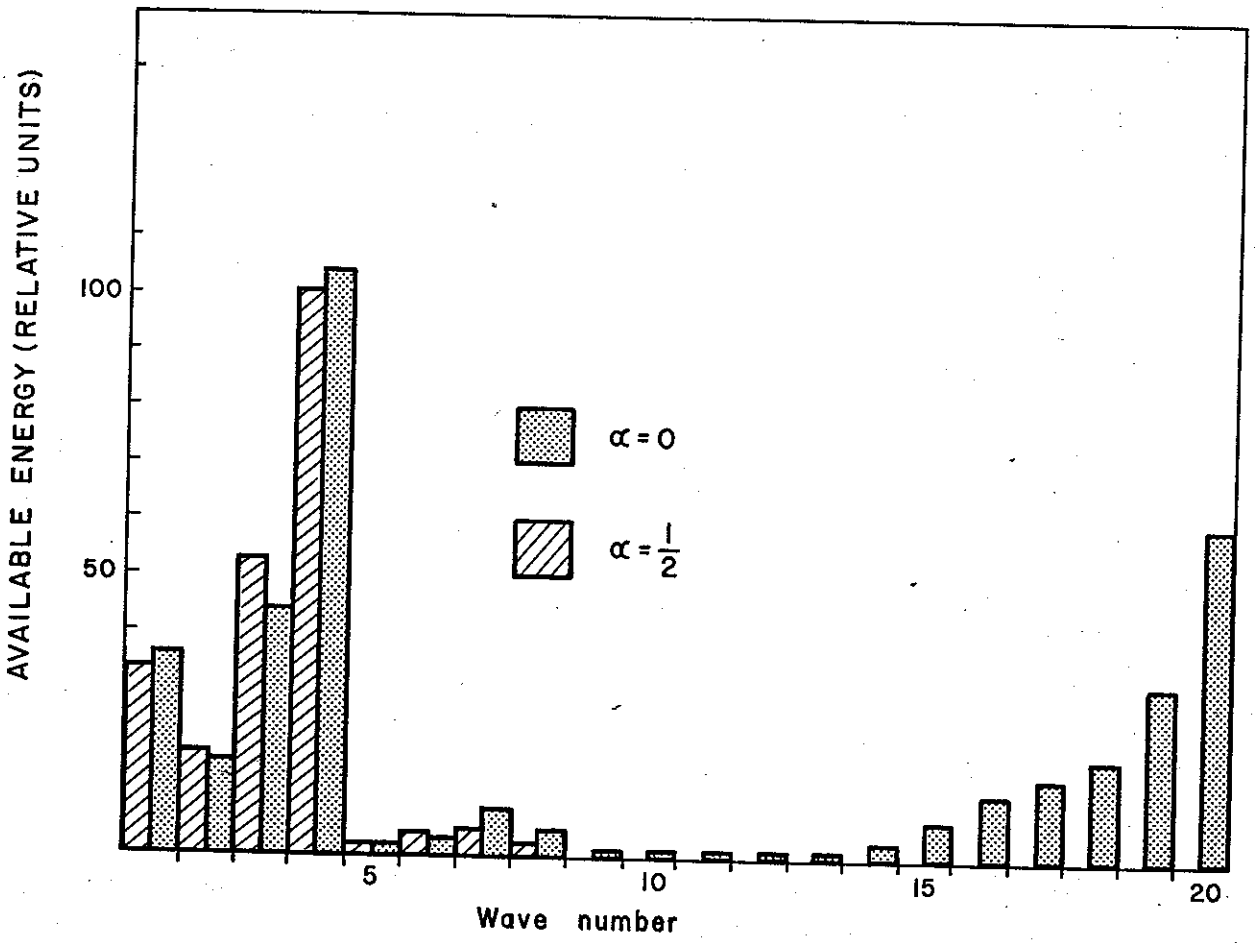

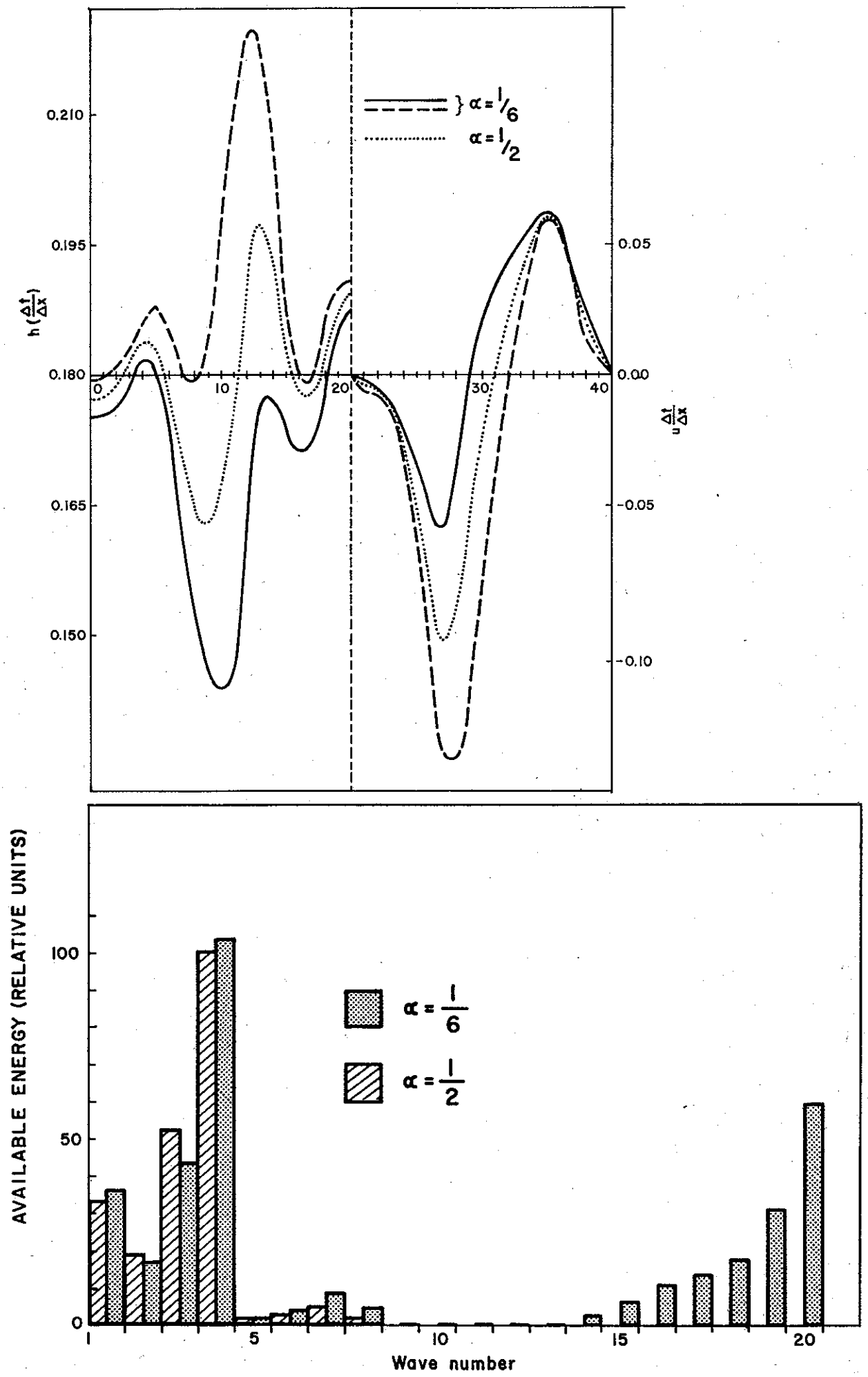

Fig. 5. (a) The potentials and velocities, and (b) the total energy distributions for $\alpha = 1/6$ and $\alpha = 1/2$ after 650 timesteps.

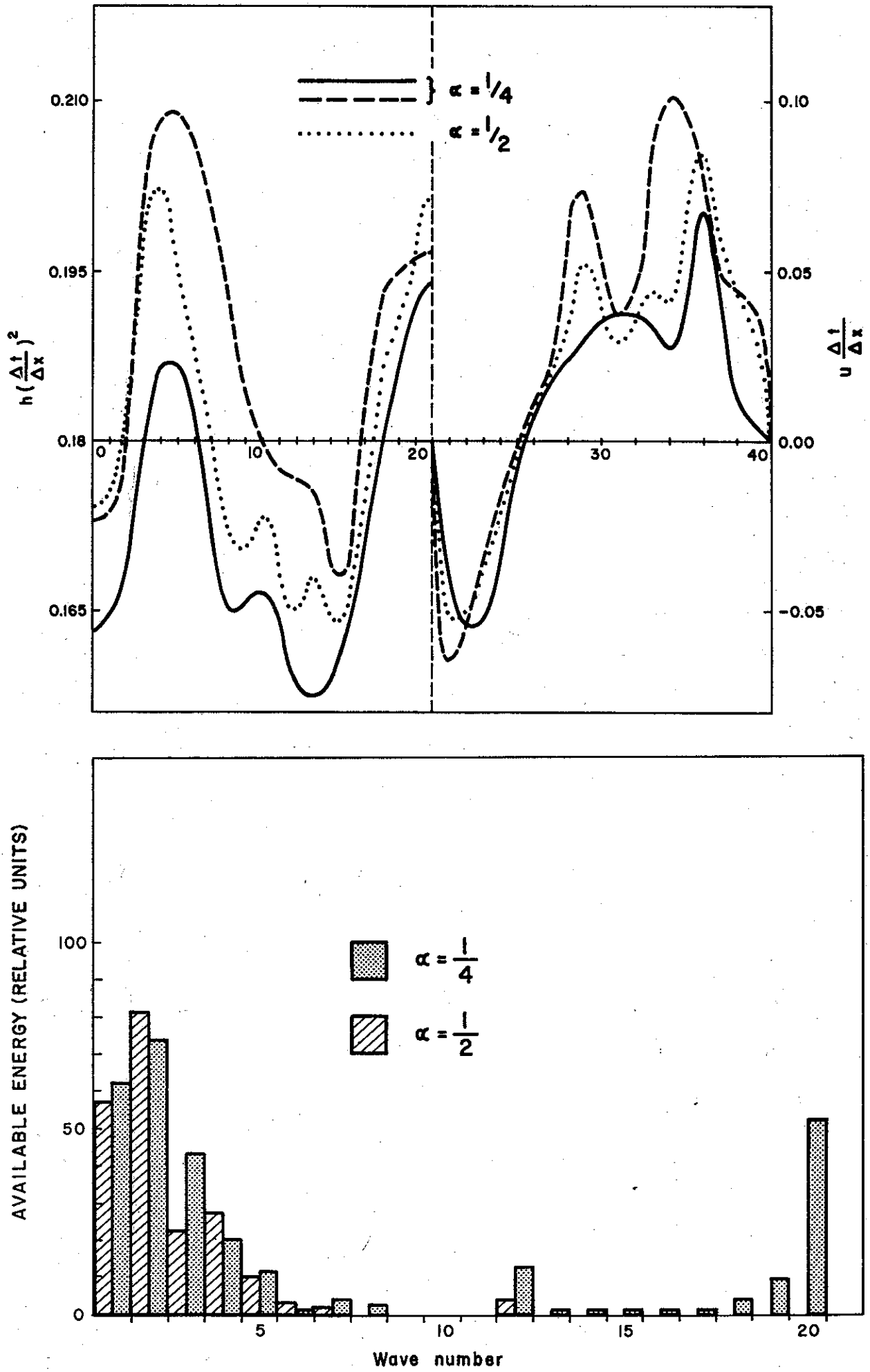

Fig. 6. (a) The potentials and velocities and (b) the total energy distributions for $\alpha = 1/4$ and $\alpha = 1/2$ after 8000 timesteps.

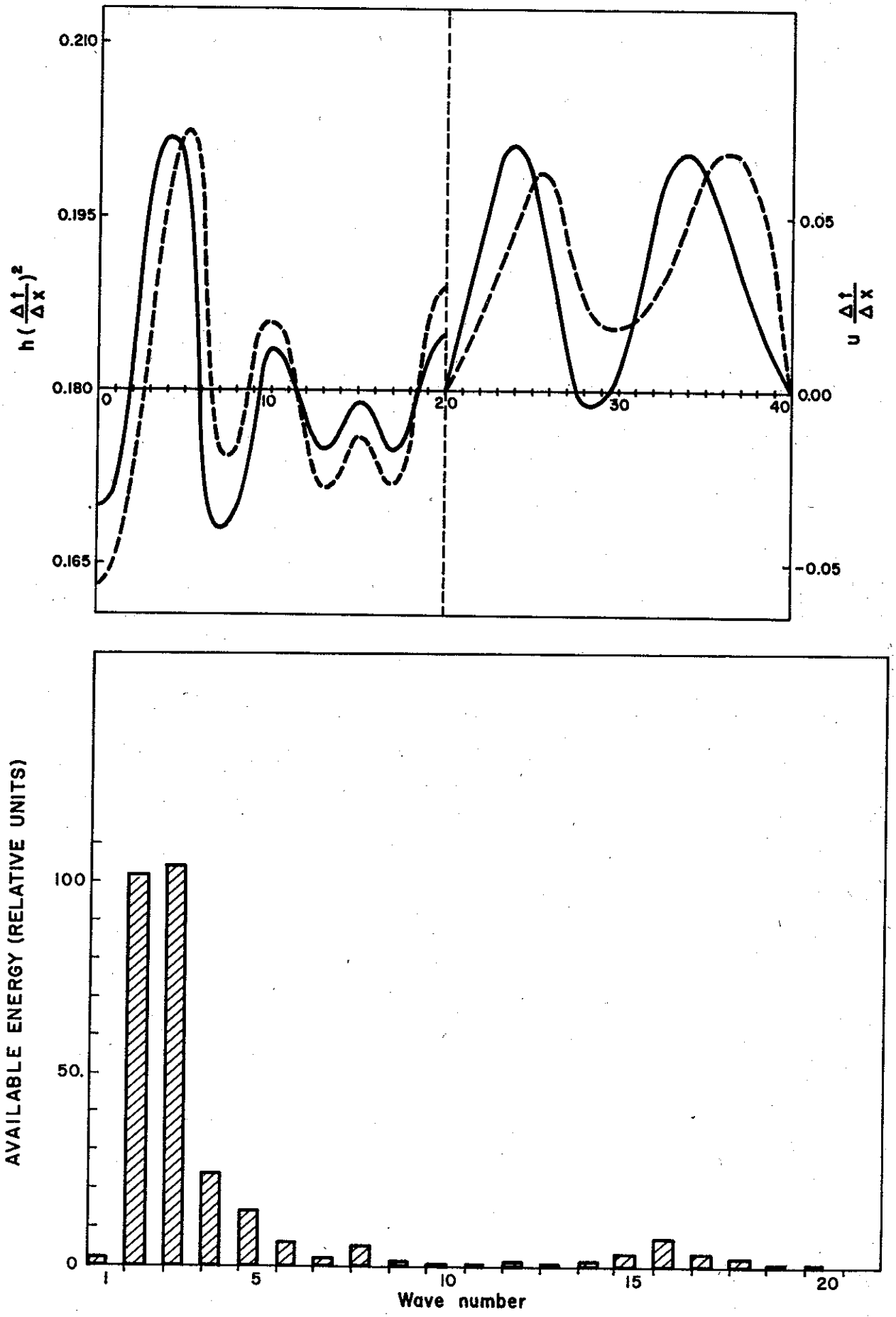

Fig. 7. (a) The potential and velocity and (b) the total energy distribution for $\alpha = 1/2$ after 18500 time-steps. (The solid curve is drawn through the even gridpoints and the broken curve through the odd gridpoints.)

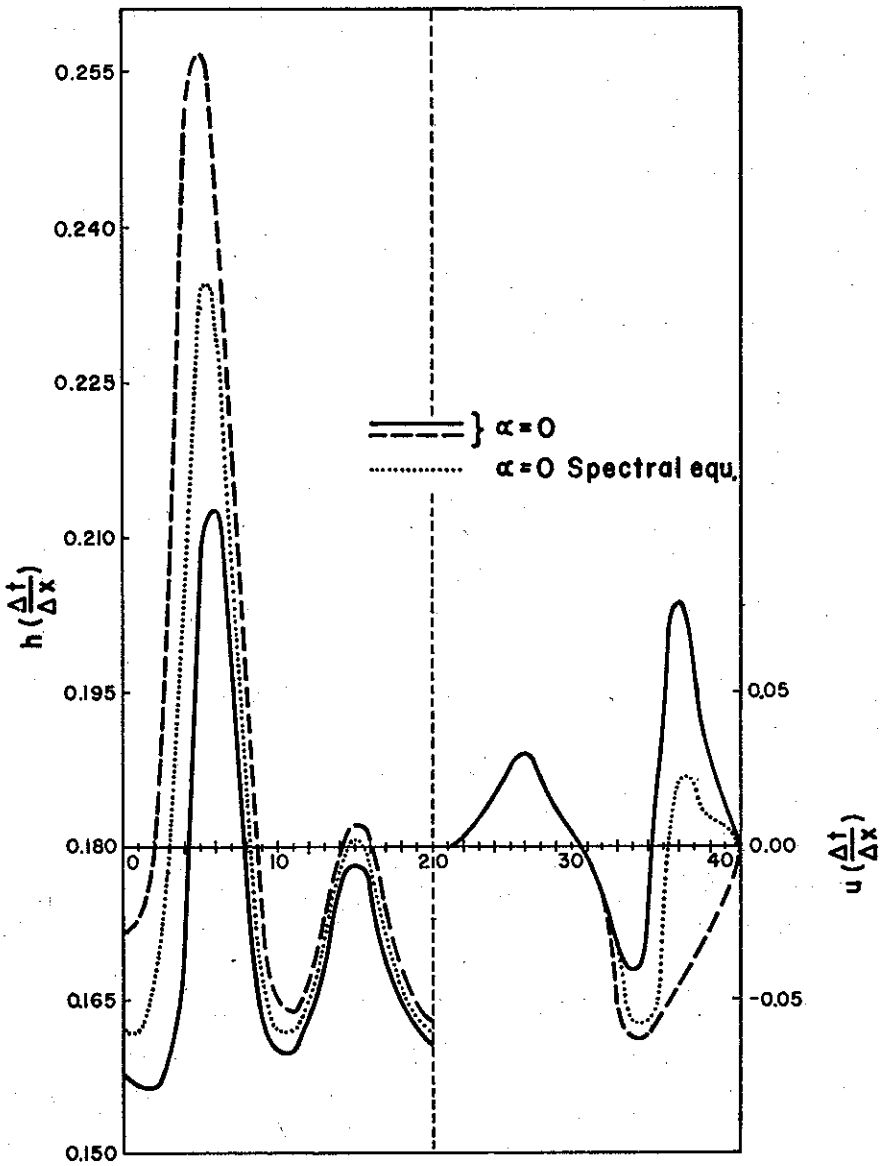

Fig. 8. (a) The potential and the velocity and (b) the total energy distribution for $\alpha = 0$ after 350 timesteps, using spectral equations without aliasing terms.

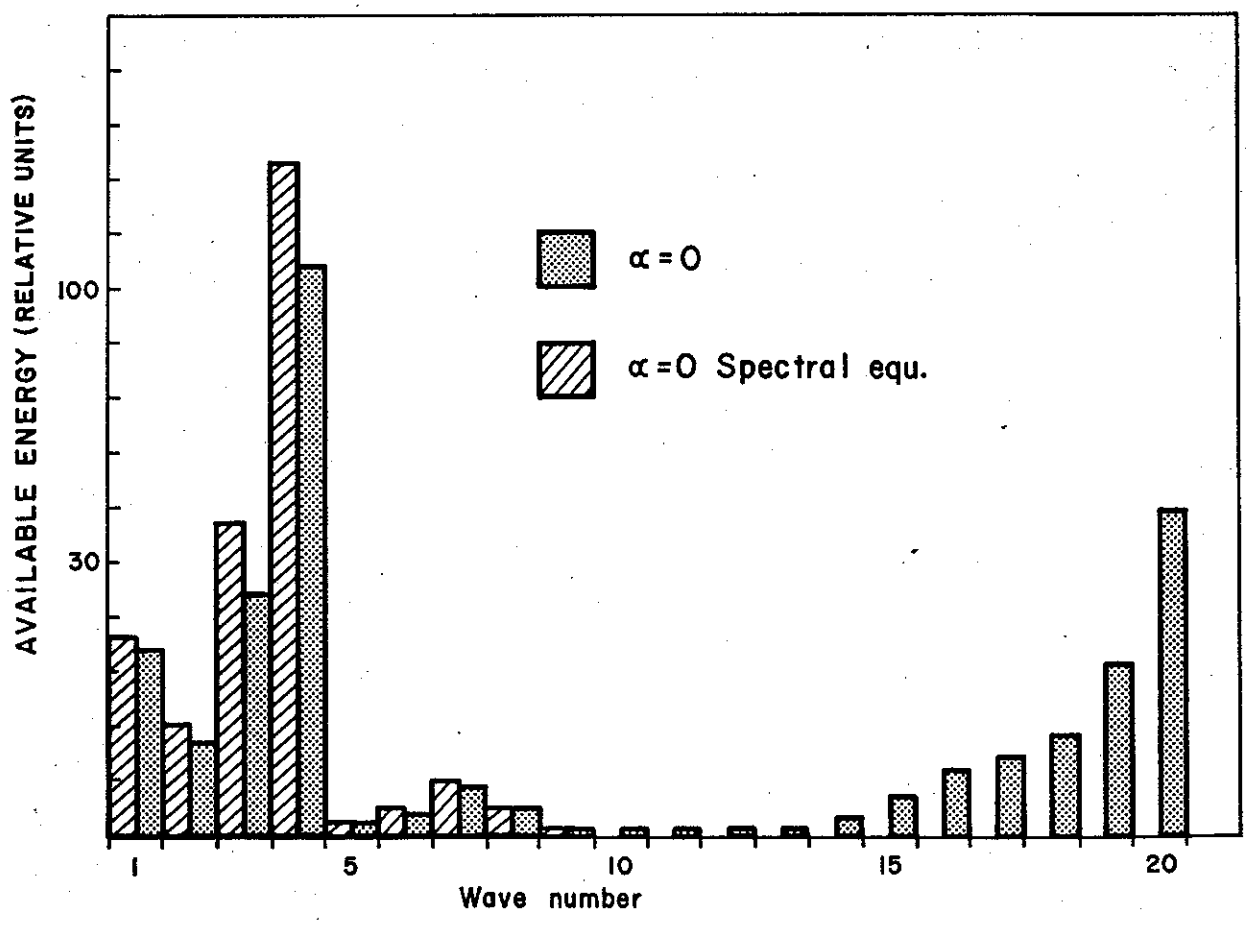

through the even grid points and the broken curve is drawn through the odd grid points, and we see that the potential and the velocity are characterized by very short waves superimposed upon long waves. The total energy distribution at the different wave numbers is shown in Fig. 4b, and this shows that the largest part of the energy is at wave numbers 1 to 4 and at wave numbers 15 to 20.

These results are compared with the results of the integration with the semi-momentum form ($\alpha = 1/2$). After 350 timesteps the results are the dotted curves in Fig. 4a, and we see that the potential h and the velocity u seem to have the same long waves as the advective form, but the short ones are missing. The same is also shown by the energy distribution in Fig. 4b. Since the integration of (3.6) and (3.7) with the advective form and the semi-momentum form gives almost the same total energy at the low wave number, the instability of the advective form has to come from the increase in total energy at the high wave numbers.

In Figs. 5 and 6 we have made the same comparison between the results of the integration of (3.6) and (3.7) with $\alpha = 1/6$ and $\alpha = 1/4$ with the results of the integration with $\alpha = 1/2$, and we get the same results that the energy at the low wave numbers is approximately equal but when the instability occurs for $\alpha = 1/6$ and $1/4$ the energy at the high wave numbers increases strongly.

If the integration with $\alpha = 1/2$ is continued for a long time, we find that the energy of some of the high wave numbers is increasing, and Fig. 7a shows the potential, h, and the velocity, u, after 18500 timesteps, where the curves are drawn separately through the even and odd gridpoints. Since there is no coupling between the even and odd grid points for $\alpha = 1/2$, we have to expect separation of the solution, and Fig. 7b shows that the separation comes from an increase of energy at wave numbers 15 to 19.

6. Integration of the spectral equations. The two main sources of error in our integrations with finite differences are due to the fact that the derivatives in space and time are approximated by truncated Taylor series with a second order accuracy and that instead of an infinite wave spectrum we have a limited wave spectrum. Let us for u_j^r and h_j^r in (3.6) and (3.7) use the following Fourier substitutions.

$$u_j^r = \sum_{n=-N}^{+N} \hat{u}_n^r e^{i(\pi/N)nj} \tag{6.1}$$

and

$$h_j^r = \sum_{n=-N}^{+N} \hat{h}_n^r e^{i(\pi/N)nj} \tag{6.2}$$

where n is the wave number. $\hat{u}_n^r$ and $\hat{h}_n^r$ are the time dependent amplitudes at wave number n, and N, as before, is the total number of waves or the highest wave number which can be represented in the model.

Introducing (6.1) and (6.2) into (3.6) with $\alpha=0$ gives us the following difference equation for the amplitude $\hat{u}_n^r$ when $n \geqslant 1$

$$\hat{u}_n^{r+1} = \hat{u}_n^{r-1} - 2i\hat{h}_n^r \sin\frac{\pi}{N}n - 2i\sum_{k=-N+n}^{N} \hat{u}_{n-k}^r \hat{u}_k^r \sin\frac{\pi}{N}k - 2i\sum_{k=-N}^{-N+(n-1)} \hat{u}_{n-(2N+k)}^r \hat{u}_k^r \sin\frac{\pi}{N}k \tag{6.3}$$

where the last term is the aliasing term, which we have to include when we have a finite wave spectrum. For a finite wave spectrum

$$e^{i(\pi/N)(n-2N)j} = e^{i(\pi/N)nj},$$

and if a wave with wave number $n-2N$ is generated it is reflected back to wave number n.

From (6.3) we also see that the nonlinear term for all $n \geqslant 1$ consists of a sum of $2N+1$ products, and that wave number 1 has no aliasing error. After some rearrangement, (6.3) may be written

$$\begin{aligned}\hat{u}_n^{r+1} = \hat{u}_n^{r-1} - 2i\hat{h}_n^r \sin\frac{\pi}{N}n - 2i\Bigg[&\sum_{k=n}^{N} \hat{u}_{n-k}^r \hat{u}_k^r \left(\sin\frac{\pi}{N}(n-k) + \sin\frac{\pi}{N}k\right) \\ &+ \tfrac{1}{2}\sum_{k=1}^{n-1} (\hat{u}_{n-k}^r \hat{u}_k^r - \hat{u}_{-N+n-k}^r \hat{u}_{-N+k}^r)\left(\sin\frac{\pi}{N}(n-k) + \sin\frac{\pi}{N}k\right)\Bigg]\end{aligned} \tag{6.4}$$

Using (3.7) the corresponding equation for $\hat{h}_j^r$ is

$$\begin{aligned}\hat{h}_n^{r+1} = \hat{h}_n^{r-1} - 2i\Bigg[&\sum_{k=n}^{N} (\hat{u}_{n-k}^r \hat{h}_k^r + \hat{u}_k^r \hat{h}_{n-k}^r)\left(\sin\frac{\pi}{N}(n-k) + \sin\frac{\pi}{N}k\right) \\ &+ \sum_{k=1}^{n-1} (\hat{u}_{n-k}^r \hat{h}_k^r - \hat{u}_{-N+n-k}^r \hat{u}_{-N+k}^r)\left(\sin\frac{\pi}{N}(n-k) + \sin\frac{\pi}{N}k\right)\Bigg]\end{aligned} \tag{6.5}$$

Since (6.4) and (6.5) are the spectral equations corresponding to (3.6) and (3.7) with $\alpha=0$, an integration of (6.4) and (6.5) with the same initial conditions will give the same results as shown in Fig. 4. To test the influence of the aliasing terms on these results, (6.4) and (6.5) are integrated without the aliasing term, and the results after 350 timesteps are shown in Fig. 8. This shows that there is no significant total energy at the high wave numbers, but the total energy at the low wave numbers is a little higher. But when the integration is continued we get a piling up of total energy at the high wave numbers, and the solution becomes unstable. The results after 550 timesteps are shown in Fig. 9. The exclusion of the aliasing terms from the advective form will not prevent instability in this model but will only delay its development.

From the initial condition used in the experiments it follows from (6.4) and (6.5) that $\hat{u}_n^r$ always is imaginary and $\hat{h}_n^r$ always is real. Therefore

$$\hat{u}_n^r = i\bar{u}_n^r = -i\bar{u}_{-n}^r \tag{6.6}$$

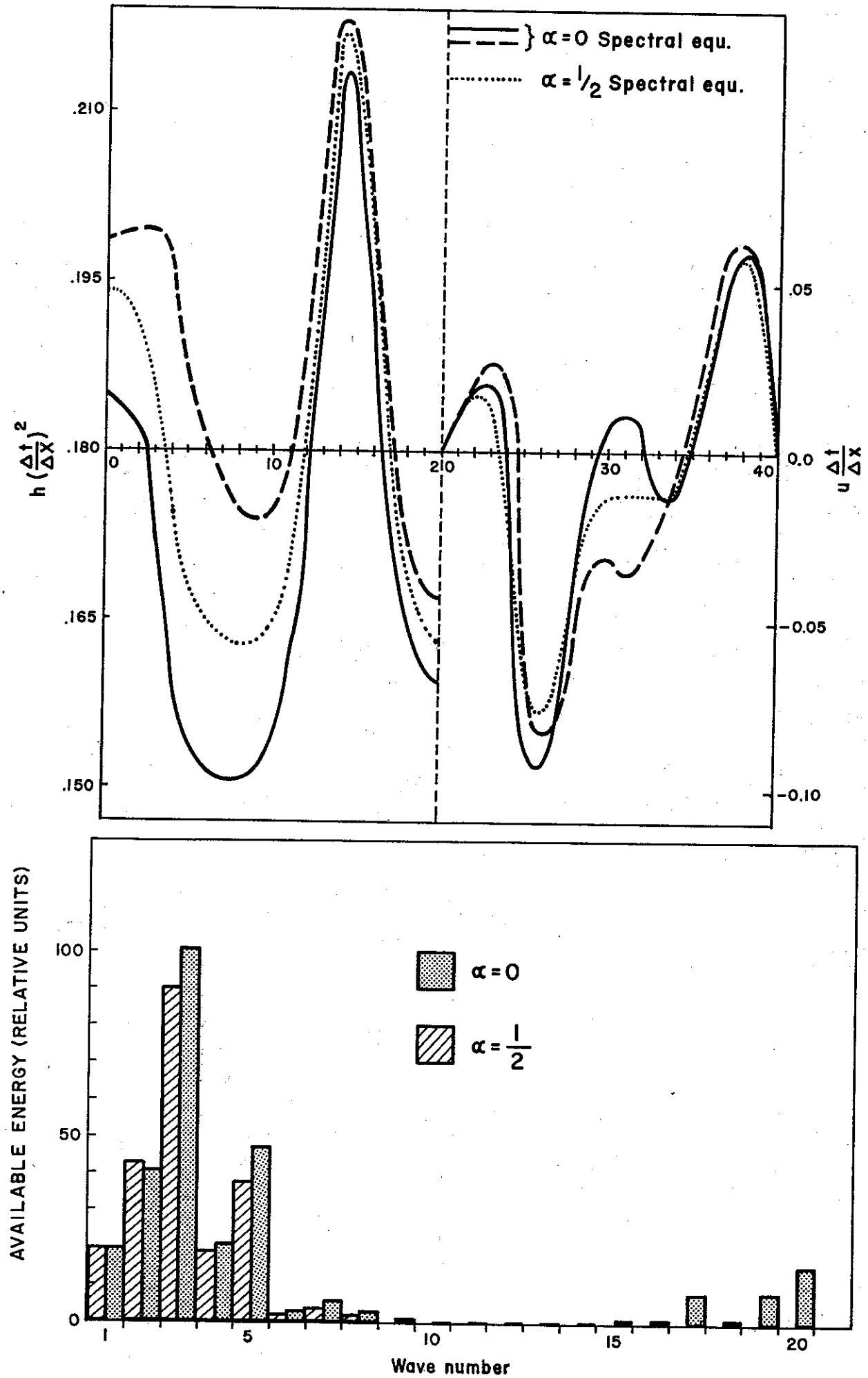

Fig. 9. (a) The potential and the velocity and (b) the total energy distribution for $\alpha = 0$ and $\alpha = 1/2$ after 550 timesteps, using spectral equations without aliasing terms.

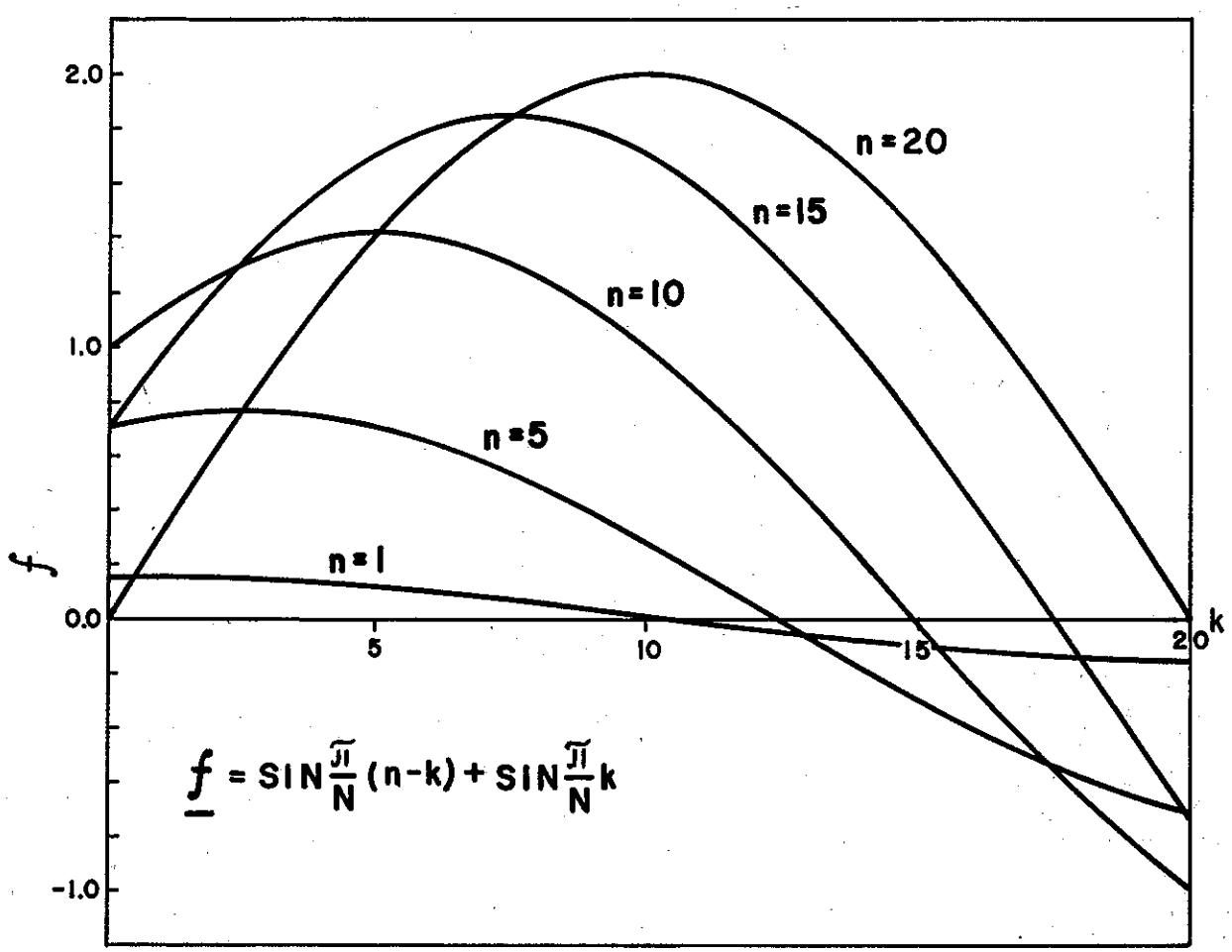

Fig. 10. $f = \sin(\pi/N)(n-k) + \sin(\pi/N)k$ for different values of n.

and

$$\hat{h}_n^r = \hat{h}_{-n}^r$$

where $\hat{u}_n^r$ is real. Putting (6.6) into (6.4) and (6.5) gives for $n=20$

$$\hat{u}_{20}^r = 0 \tag{6.7}$$

and

$$\hat{h}_{20}^{r+1} = \hat{h}_{20}^{r-1} + 8 \sum_{k=1}^{19} \hat{u}_{20-k}^r \hat{h}_k^r \sin \frac{\pi}{N} k \tag{6.8}$$

If the aliasing term is excluded from (6.5) the only change in (6.8) is that we only get half of the last term.

If the absolute value of $\hat{h}_{20}^{r+1}$ is bounded and the solution stable, the correlation between $\hat{h}_{20}^{r-1}$ and the sum in (6.8) must be negative. There is, however, no reason to expect this, and in this integration the correlations are positive with a generation or transport of energy to the high wave numbers.

If the velocity u_j^r and the potential h_j^r are expanded in infinite Fourier series (continuous space),

$$u_j^r = \sum_{n=-\infty}^{+\infty} \hat{u}_n^r e^{i(/\pi N)nj}$$

$$h_j^r = \sum_{n=-\infty}^{+\infty} \hat{h}_n^r e^{i(\pi/N)nj}, \tag{6.9}$$

the spectral equations corresponding to (2.4) and (2.5) are, when dimensionless variables are used,

$$\frac{\partial \hat{u}_n^r}{\partial t} = -i\frac{\pi n}{N}\left[\hat{h}_n^r + \sum_{k=n}^{\infty} \hat{u}_{n-k}^r \hat{u}_k^r + \tfrac{1}{2}\sum_{k=0}^{n-1} \hat{u}_{n-k}^r \hat{u}_k^r\right] \tag{6.10}$$

$$\frac{\partial \hat{h}_n^r}{\partial t} = -i\frac{\pi}{N}n\left[\sum_{k=n}^{\infty} (\hat{u}_{n-k}^r \hat{h}_k^r + \hat{u}_k^r \hat{h}_{n-k}^r) + \sum_{k=0}^{n-1} \hat{u}_{n-k}^r \hat{u}_k^r\right] \tag{6.11}$$

In (6.10) and (6.11) the aliasing terms are missing, and instead of $\sin(\pi/N)n$ and $(\sin(\pi/N)(n-k)+\sin(\pi/N)k)$ in (6.4) and (6.5) we have the wave number $(\pi/N)n$.

The value of $(\sin(\pi/N)(n-k)+\sin(\pi/N)k)$ for different values of n is given in Fig. 10.

For $k \leq n$,

$$\left(\sin\frac{\pi}{N}(n-k) + \sin\frac{\pi}{N}k\right)$$

is a better approximation to $(\pi/N)n$ then $\sin(\pi/N)n$, but when $k>n$ the approximation is less, and for $k>(N+n)/2$ its value becomes negative. To avoid this misrepresentation, which is greatest at the low wave numbers, $\hat{u}_n^r$ and $\hat{h}_n^r$ have to be small for $n>(N/2)$.

To get a stable solution and a right representation of the low wave numbers the amplitudes of the high wave numbers have, therefore, to be damped. Multiplying the sums in (6.4) and (6.5) with $\sin^2(\pi/N)n$ when $n>(N/2)$ seems to give a stable solution, but the integration was not performed for more than 2000 timesteps. A multiplication with $\sin(\pi/N)n$ did not give a sufficient dampening and the solution became unstable.

Integration of (3.6) and (3.7) shows that to get a solution which behaves stably for more than 800 timesteps we have to choose $\alpha \geq 1/4$, and the semi-momentum form, $\alpha=1/2$, gives the most stable solution. The spectral equations corresponding to (3.6) and (3.7) with $\alpha=1/2$ are

$$\hat{u}_n^{r+1} = \hat{u}_n^{r-1} - 2i\sin\frac{\pi}{N}n\left[\hat{h}_n^r + \sum_{k=n}^{N} \hat{u}_{n-k}^r \hat{u}_k^r + \tfrac{1}{2}\sum_{k=1}^{n-1} (\hat{u}_{n-k}^r \hat{u}_k^r + \hat{u}_{-N+n-k}^r \hat{u}_{-N+k}^r)\right] \tag{6.12}$$

$$\hat{h}_n^{r+1}=\hat{h}_n^{r-1}-2i\sin\frac{\pi}{N}n\left[\sum_{k=n}^{N}(\hat{u}_{n-k}^r\hat{h}_k^r+\hat{u}_k^r\hat{h}_{n-k}^r)+\sum_{k=1}^{n-1}(\hat{u}_{n-k}^r\hat{h}_k^r+\hat{u}_{-N+n-k}^r\hat{h}_{-N+k}^r)\right] \tag{6.13}$$

The wave number $(\pi/N)n$ is in these equations approximated by $\sin(\pi/N)n$, which will damp $\hat{u}^{r+1}_n$ and $\hat{h}^{r+1}_n$ strongly when $n>N/2$, and compared to (6.4) and (6.5) the aliasing terms have changed sign. Since the aliasing terms in (6.4) and (6.5) seem to make the solution more unstable, they should in (6.12) and (6.13) act to stabilize the solution. If the amplitudes $\hat{u}^r_n$ and $\hat{h}^r_n$ are small for $n>N/2$, the aliasing terms at the wave numbers $n>N/2$ also become small, and when N is large, the semi-momentum form should for the lowest wave numbers, except for time truncations, give a good approximation to the real solution.

The other difference forms which are used are a combination of the advective form and the semi-momentum form. Using (6.1) gives

$$u_j^r+\alpha(u_{j+1}^r+u_{j-1}^r-2u_j^r)=\sum_{n=-N}^{N}\hat{u}_n^r\left[(1-2\alpha)+2\alpha\cos\frac{\pi}{N}n\right]e^{i\pi/Nn}, \tag{6.14}$$

and we see that the filter factor form, $\alpha=1/4$, for example, is the arithmetic mean between the advective form and the semi-momentum form. If the advective form is unstable, we also have to expect the other difference forms with $\alpha<1/2$ to be unstable.

If a staggered grid is used only one of the solutions in Fig. 7 is obtained, but the aliasing terms are now formed by reflection of waves with wave number $n>N/2$ back to wave number $-N+n$. From

$$e^{i(\pi/N)nj}=(-1)^je^{i\pi/N(-N+n)}$$

follows that the aliasing terms will change sign for every timestep when we are shifting between the even and odd grid points, and the solution will get this single timestep oscillation.

7. Concluding remarks. The experiments with this model show that only the semi-momentum form may give a computationally stable solution, when the gravity oscillations are not completely damped out.

The semi-momentum form contains non-linear friction or smoothing which will prevent rapid increase of energy at the shortest waves, and the aliasing terms become small as long as the amplitudes of the shortest waves are small. It is not only the aliasing terms which make the other difference schemes unstable but also the approximation to the wave number $(\pi/N)n$ in the non-linear terms.

To damp the high frequency oscillations in time and the separation of the solution in the long time integration, it is necessary to include an artificial friction term in the equations also when the semi-momentum form is used.

REFERENCES

ARAKAWA, A. 1963: Computational design for long term numerical integrations of the equations of atmospheric motion. Paper presented at 44th annual meeting, *American Geophysical Union*, Washington D.C.

BRYAN, K. 1966: A scheme for numerical integration of the equation of motion on an irregular grid free of non-linear instability. *Mon. Wea. Rev.* **94**, 39.

ELIASSEN, A. 1964: On numerical integration of certain partial differential equations by means of the "improved Euler-Cauchy method". Part II, Final Report. Contract AF 61(052)—525. Inst. for Geofysikk, Universitetet i Oslo.

HOUGHTON, D., A. KASAHARA, & W. WASHINGTON, 1966: Long-term integration of the barotropic equations by the Lax-Wendroff method. *Mon. Wea. Rev.* **94**, 141.

LAX, P. D. & B. WENDROFF, 1960: Systems of conservation laws. *Com. on Pure and Appl. Math.* **13**, 217.

LILLY, D. K., 1965: On the computational stability of numerical solutions of time-dependent, non-linear geophysical fluid dynamics problems. *Mon. Wea. Rev.* **93**, 11.

MIYAKODA, K., 1962: Contribution to numerical weather prediction-computation with finite difference. *Japanese J. of Geoph.* **3**, 75.

PHILLIPS, N. A., 1959: An example of non-linear computational instability. *The Atmosphere and Sea in Motion*, Rockefeller Institute Press and Oxford University Press, N.Y., p. 50.

SHUMAN, F. G., 1957: Numerical methods in weather prediction: II. Smoothing and filtering. *Mon. Wea. Rev.*, **85**, 357.

— 1960: Numerical experiment with primitive equations. *Proc. Int. Sym. Num. Weather Pred. in Tokyo, Nov. 11—13, 1960.* Meteorological Society of Japan 1962, p. 85.

Avhandlinger som ønskes opptatt i «Geofysiske Publikasjoner», må fremlegges i Videnskaps-Akademiet av et sakkyndig medlem.

Vol. XXII.

No. 1. L. Harang and K. Malmjord: Drift measurements of the E-layer at Kjeller and Tromsø during the international geophysical year 1957—58. 1960.
» 2. Leiv Harang and Anders Omholt: Luminosity curves of high aurorae. 1960.
» 3. Arnt Eliassen and Enok Palm: On the transfer of energy in stationary mountain waves. 1961.
» 4. Yngvar Gotaas: Mother of pearl clouds over Southern Norway, February 21, 1959. 1961.
» 5. H. Økland: An experiment in numerical integration of the barotropic equation by a quasi-Lagrangian method. 1962.
» 6. L. Vegard: Auroral investigations during the winter seasons 1957/58—1959/60 and their bearing on solar terrestrial relationships. 1961.
» 7. Gunnvald Bøyum: A study of evaporation and heat exchange between the sea surface and the atmosphere. 1962.

Vol. XXIII.

No. 1. Bernt Mæhlum: The sporadic E auroral zone. 1962.
» 2. Bernt Mæhlum: Small scale structure and drift in the sporadic E layer as observed in the auroral zone. 1962.
» 3. L. Harang and K. Malmjord: Determination of drift movements of the ionosphere at high latitudes from radio star scintillations. 1962.
» 4. Eyvind Riis: The stability of Couette-flow in non-stratified and stratified viscous fluids. 1962.
» 5. E. Frogner: Temperature changes on a large scale in the arctic winter stratosphere and their probable effects on the tropospheric circulation. 1962.
» 6. Odd H. Sælen: Studies in the Norwegian Atlantic Current. Part II: Investigations during the years 1954—59 in an area west of Stad. 1963.

Vol. XXIV.

In memory of Vilhelm Bjerknes on the 100th anniversary of his birth. 1962.

Vol. XXV.

No. 1. Kaare Pedersen: On the quantitative precipitation forecasting with a quasi-geostrophic model. 1963.
» 2. Peter Thrane: Perturbations in a baroclinic model atmosphere. 1963.
» 3. Eigil Hesstvedt: On the water vapor content in the high atmosphere. 1964.
» 4. Torbjørn Ellingsen: On periodic motions of an ideal fluid with an elastic boundary. 1964.
» 5. Jonas Ekman Fjeldstad: Internal waves of tidal origin. 1964.
» 6. A. Eftestøl and A. Omholt: Studies on the excitation of N_2 and N_2^+ bands in aurora. 1965.

Vol. XXVI.

No. 1. Eigil Hesstvedt: Some characteristics of the oxygen-hydrogen atmosphere. 1965.
» 2. William Blumen: A random model of momentum flux by mountain waves. 1965.
» 3. K. M. Storetvedt: Remanent magnetization of some dolerite intrusions in the Egersund Area, Southern Norway. 1966.
» 4. Martin Mork: The generation of surface waves by wind and their propagation from a storm area. 1966.
» 5. Jack Nordø: The vertical structure of the atmosphere. 1965.
» 6. Alv Egeland and Anders Omholt: Carl Størmer's height measurements of aurora. 1966.
» 7. Gunnvald Bøyum: The energy exchange between sea and atmosphere at ocean weather stations M, I and A. 1966.
» 8. Torbjørn Ellingsen and Enok Palm: The energy transfer from submarine seismic waves to the ocean. 1966.
» 9. Torkild Carstens: Experiments with supercooling and ice formation in flowing water. 1966.
» 10. Jørgen Holmboe: On the instability of stratified shear flow. 1966.
» 11. Lawrence H. Larsen: Flow over obstacles of finite amplitude. 1966.

A.s John Griegs Boktrykkeri